Functional Magnetic Resonance Imaging

11

Zhongming Liu and Jiayue Cao

Abstract

Functional magnetic resonance imaging has become a primary tool for psychological and cognitive studies or preclinical brain research. As a technique to map brain function, fMRI measures the blood oxygenation level–dependent signal as a collective effect of changes in cerebral blood flow, cerebral blood volume, and cerebral metabolic rate of oxygen following changes in neural activity. The use of fMRI in combination with carefully designed task paradigms has enabled scientists to map perceptual, cognitive, or behavioral functions onto brain regions and networks. Spontaneous activity observed with fMRI in task-free resting states has been used to reveal intrinsic functional networks that collectively depict the brain's functional architecture or connectome. Naturalistic paradigms for fMRI are increasingly used to map brain activation, address neural representation and coding, and characterize brain networks while humans are engaged in a realistic and dynamic environment similar to daily life experiences. In this chapter, we discuss the principles, methods, and applications of fMRI, with emphasis on its biophysical and physiological basis, experimental designs and analysis methods, and applications to human and animal studies. Example data or results from empirical studies are presented to help illustrate methods or support scientific views.

Keywords

Nuclear magnetic resonance · Longitudinal relaxation · Transverse relaxation · Hemoglobin · Magnetic susceptibility · Blood oxygenation level dependent · Neurovascular coupling · Hemodynamic response function · Statistical parametric mapping · Resting state networks · Functional connectivity · Naturalistic paradigm

11.1 Introduction

To study how the brain works, it is desirable to image neural activity throughout the brain while being able to see every neuron and detect every neuronal spike. This requires an imaging technique to have high spatial resolution, high temporal resolution, and whole-brain coverage. Unfortunately, such a technique is unavailable to

Z. Liu (✉)
Department of Biomedical Engineering, University of Michigan, Ann Arbor, MI, USA

Department of Electrical Engineering and Computer Science, University of Michigan, Ann Arbor, MI, USA
e-mail: zmliu@umich.edu

J. Cao
Department of Biomedical Engineering, University of Michigan, Ann Arbor, MI, USA

B. He (ed.), *Neural Engineering*, https://doi.org/10.1007/978-3-030-43395-6_11

date for human brain imaging, in part because for human applications it is also desirable to refrain from using any invasive procedure.

Every technique has its pros and cons and continues to progress on its own or in combination with other techniques [1]. Among all that is currently available, *functional magnetic resonance imaging* (fMRI) stands out with notable advantages by providing sub-millimeter spatial resolution, sub-second temporal resolution, and whole-brain coverage. In the past three decades, fMRI has undergone rapid development and has become a primary tool for human psychological and cognitive studies, as well as preclinical (animal) brain research.

In this chapter, we discuss fMRI with special emphasis on its biophysical and physiological basis, experimental designs and analysis methods, and applications to human and animal studies. To facilitate discussions, we include, as relevant examples, some data from our prior studies. In addition, this chapter is not intended to serve as a comprehensive literature review, and the reference list is only meant to provide additional, but not inclusive, materials to guide interested readers.

11.2 Magnetic Resonance Imaging

As the name suggests, fMRI uses *magnetic resonance imaging* (MRI) to measure brain activity and map brain functions. The physics underlying MRI is *nuclear magnetic resonance* (NMR). It describes the magnetic behavior of any atomic nucleus that has an odd number of protons. Because the human brain has high water content, the *hydrogen atom* (^{1}H), which consists of a single proton and carries a positive charge, is the most abundant nucleus for MRI. Although other nuclei, e.g., ^{13}C, ^{31}P, ^{23}Na, and ^{19}F, are also visible to MRI, fMRI is nearly all based on ^{1}H MRI. Hereafter, we refer to hydrogen atoms simply as protons, unless they are explicitly specified otherwise.

A proton spins about itself and creates a magnetic moment. It is perhaps convenient to think of a spinning proton (or a spin in short) as a tiny magnet (Fig. 11.1a). Spins in a spatial element, typically referred to as a voxel, form a spin system. In the absence of any external magnetic field, the spins in a spin system behave like many small magnets oriented in random directions (Fig. 11.1b). The magnetic fields generated by individual spins sum to zero.

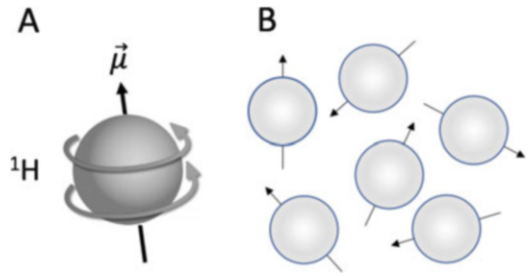

Fig. 11.1 Hydrogen protons in the absence of external magnetic field. (**a**) The spin of a single ^{1}H generates a small magnetic field $\vec{\mu}$. (**b**) Spins are randomly oriented

When an external magnetic field $\mathbf{B}_0$ is present or applied, the spins in a spin system exhibit a weak tendency to *precess* (i.e., a gyroscopic motion) along the direction of the external field, giving rise to very small net magnetization in a direction parallel to $\mathbf{B}_0$ (Fig. 11.2). Such precession has a characteristic frequency ω_0, called the *Larmor frequency*, which is proportional to $\mathbf{B}_0$ by a fixed ratio γ, called the *gyromagnetic ratio*. For ^{1}H, the gyromagnetic ratio is 42.58 MHz/Tesla. The precession (or Larmor) frequency is about 128 MHz for an MRI system operating under a 3 Tesla static magnetic field, and it is about 300 MHz for 7 Tesla MRI. Under typical field strengths, the precession frequency is always in the radio frequency (RF) range. As a spin is precessing, it creates a rotating magnetic field in the *transverse plane*, which is perpendicular to $\mathbf{B}_0$. However, spins precess with random phases; as a result, the sum of their transverse magnetization is still equal to zero (Fig. 11.2).

For a spin system to generate detectable magnetic fields in the transverse plane, it needs to receive a brief *RF excitation* – a rotating magnetic field applied to the transverse plane by using an RF transmitter (Fig. 11.3). When the RF excitation uses the same frequency as the precession frequency, i.e., *on resonance*, the spin system

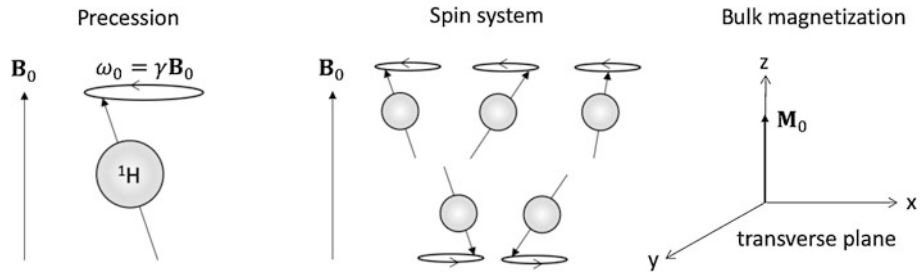

Fig. 11.2 Spins in an external magnetic field $\mathbf{B}_0$. Every spin precesses at the same frequency but with a different phase. More spins align parallel to $\mathbf{B}_0$ than antiparallel to $\mathbf{B}_0$. Of the bulk magnetization, the longitudinal component is non-zero, but the transverse component is zero

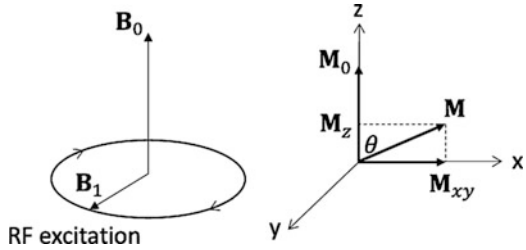

Fig. 11.3 Spins given on resonance excitation. An RF excitation $\mathbf{B}_1$ is an applied magnetic field rotating in the transverse plane (left). The excitation flips the bulk magnetization toward the transverse plane by a *flip angle* θ

effectively absorbs the energy from the excitation and progressively synchronizes the phases of individual spins while progressively reducing the longitudinal magnetic field. During the course of the excitation, the bulk magnetization that arises from the spin system is flipped down toward the transverse plane while rotating about $\mathbf{B}_0$ (Fig. 11.3).

Once the excitation is off, the longitudinal magnetization progressively returns to its thermal equilibrium, showing an approximately exponential recovery, namely, the *longitudinal relaxation*. The recovery of longitudinal magnetization is governed by a time constant T_1. A shorter T_1 means a faster longitudinal relaxation (Fig. 11.4). In the meantime, the spin system progressively desynchronizes the phases of individual spins. During dephasing, the transverse component of the bulk magnetization can be detected by an RF receiver. The detected signal shows an approximately exponential decay to zero, namely, the *transverse relaxation*. The transverse relaxation is also governed by a time constant, namely, T_2 when the magnetic field is homogeneous within the spin system or T_2* when it is inhomogeneous. A shorter T_2 or T_2* means a faster transverse relaxation (Fig. 11.4). As T_1, T_2, and T_2* are all tissue-specific properties, the signals detected by the RF receiver can report various tissue contrasts, depending on the pulse sequence used to transmit, encode, and receive the RF signals to/from spins in the brain.

For the scope of this chapter, it only covers the basic physics of MRI as the prerequisite for learning fMRI. For more comprehensive discussions about MRI, we refer the readers to other materials [2–4].

11.3 Blood Oxygenation Level–Dependent Contrast

One type of tissue contrast observable with MRI is *blood oxygenation level dependent* (BOLD) [5]. In the brain, cerebral vasculature circulates blood to supply oxygen, glucose, and nutrients. *Hemoglobin* (i.e., red blood cell) is the primary carrier of oxygen. Arteries deliver *oxygenated hemoglobin*. Oxygen is extracted from capillaries and consumed by brain tissues, creating *deoxygenated hemoglobin*. Veins drain the deoxygenated hemoglobin, along with other metabolic products.

Hemoglobin is diamagnetic when oxygenated but paramagnetic when deoxygenated [6]. With only oxygenated hemoglobin, the magnetic susceptibility of blood is nearly identical to that of

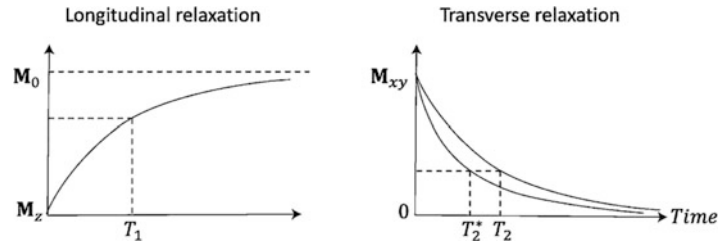

Fig. 11.4 Longitudinal (left) or transverse (right) relaxation as an exponential recovery or decay characterized by a time constant T_1, T_2, or T_2*

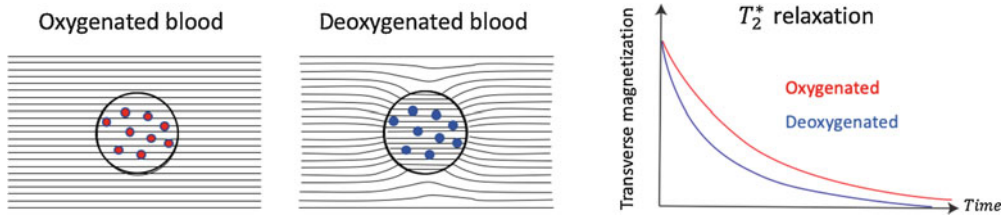

Fig. 11.5 Deoxygenated blood distorts the static magnetic field, but oxygenated blood does not. Deoxygenated blood causes a shorter T_2* than does oxygenated blood. Large circles indicate blood vessels. Small circles indicate oxygenated (red) or deoxygenated (blue) hemoglobin

brain tissue. As a result, a voxel that contains blood and tissue tends to experience a homogeneous magnetic field. With only deoxygenated hemoglobin, the blood susceptibility mismatches the tissue susceptibility, distorting the magnetic field into an inhomogeneous distribution. The blood in a voxel includes a varying mixture of oxygenated and deoxygenated hemoglobin. Higher concentration of deoxygenated hemoglobin results in greater distortion to the magnetic field and causes the spins in the voxel to experience more distinct magnetic fields such that they precess with more distinct frequencies [7]. As a result, spins tend to run out of synchronization faster, while faster dephasing results in shorter T_2* and faster transverse relaxation (Fig. 11.5).

When reading out the T_2*-weighted signal at an echo time close to T_2*, the signal magnitude is negatively dependent on the concentration of deoxygenated hemoglobin or positively dependent on the concentration of oxygenated hemoglobin. The latter has been more commonly used for interpretation of fMRI and has been conventionally termed as BOLD since a seminal paper by Ogawa et al. [5]. In short, the BOLD signal is higher when the concentration of oxygenated hemoglobin increases or when the concentration of deoxygenated hemoglobin decreases [8].

11.4 BOLD Response to Neural Activity

Functional MRI uses the BOLD signal to localize neural activity [9–11]. The precise relationship between the BOLD signal and neural activity is not fully understood and still under active research. Nevertheless, evidence from prior studies has shed light onto the biophysical basis and physiological origin of the BOLD signal [12, 13]. Here, we discuss the understanding that has received general consensus.

Neural activity requires energy and consumes oxygen. Elevation of neural activity (or activation) triggers a cascade of metabolic and hemodynamic events, collectively contributing to the BOLD signal. As illustrated in Fig. 11.6, at an activated region, more oxygen is extracted and consumed, giving rise to an increase in the *cerebral metabolic rate of oxygen* ($CMRO_2$). The brain reacts to the increasing demand and consumption of oxygen by actively dilating arterioles and capillaries to allow more oxygenated blood

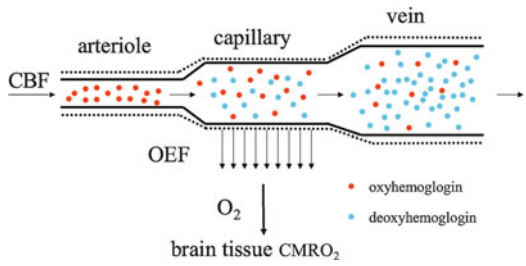

Fig. 11.6 Neural activation causes oxygen consumption to increase, arterioles to dilate, capillaries and veins to expand, both blood flow and volume to increase, and the BOLD signal to rise. Solid and dashed lines indicate the blood vessels before and after neural activation, respectively. OEF, oxygen extraction fraction, indicates the fraction of oxygen extracted from the bloodstream and supplied to brain tissue

to flow into the activated region. The upstream increase in blood flow causes a passive expansion of the downstream venioles or veins, similar to draining water through a balloon [14]. As such, both *cerebral blood volume* (CBV) and *cerebral blood flow* (CBF) increase given elevated neural activity.

Importantly, the increase in CBF overcompensates for the increase in $CMRO_2$ [15]. The brain supplies more blood to deliver more oxygen than is consumed by neural activity. This effect leads to increase in the concentration of oxygenated hemoglobin or decrease in the concentration of deoxygenated hemoglobin, causing the BOLD signal to increase. To capture this signal with MRI, such pulse sequences as echo-planar imaging [16] or spiral imaging [17, 18] are often used for fast imaging with T_2*-weighted contrast. Recent advances in RF coils, pulse sequences, and image reconstruction have contributed to further acceleration to enable whole-brain fMRI within 1 s [19, 20].

How neural activity drives hemodynamic changes (i.e., *neurovascular coupling*) is not precisely understood [21]. Evidence suggests that active dilation of blood vessels is not directly controlled by neurons but mediated through astrocytes [22]. Hemodynamic responses are more driven by and coupled to synaptic inputs to neurons, rather than spiking output from neurons [23]. In part for this reason, the BOLD signal is more observable in the brain's gray matter than in the white matter, although findings from recent studies suggest the feasibility of using BOLD fMRI to map white matter functions [24–26].

11.5 Hemodynamic Response Function

Although the physiological mechanism of neurovascular coupling is not fully clear, models have been derived from empirical data in an attempt to mathematically describe the relationship between neural activity and its resulting hemodynamic response [23, 27, 28]. Neurovascular coupling is considered as a linear time-invariant system, for which neural activity is the input and vascular response is the output. In line with the established notion of linear systems, the model of neurovascular coupling is often described as a *hemodynamic impulse response function*, which describes the system's output given an impulse input, i.e., a delta function. In literature, the hemodynamic impulse response function is called the hemodynamic response function (HRF). Despite the omission of "impulse", it is worth emphasizing that the HRF should be interpreted as the vascular response to an impulse neural input.

The HRF is typically modeled as the sum of two gamma functions. Many software tools for fMRI analysis have implemented the HRF, e.g., the MATLAB-based SPM software. Parameters that control the shape of the HRF include the latencies and durations. With the default parameters, the HRF is called the canonical HRF (Fig. 11.7), in which the impulse response reaches the positive peak at 5 s, returns to baseline (zero) at 12 s, undershoots at about 15 s, and again returns to baseline at about 25 s. Clearly, the HRF is very slow and behaves like a low-pass filter with an (arguably conservative) cutoff frequency at 0.2 Hz. For this reason, the BOLD signal is not rapid enough to follow fast modulation of neural activity – a notable limitation of fMRI. That said, the bandwidth of the BOLD signal is still debatable, as recent findings demonstrate the feasibility of detecting neurogenic BOLD responses as fast as 0.8 Hz [29, 30].

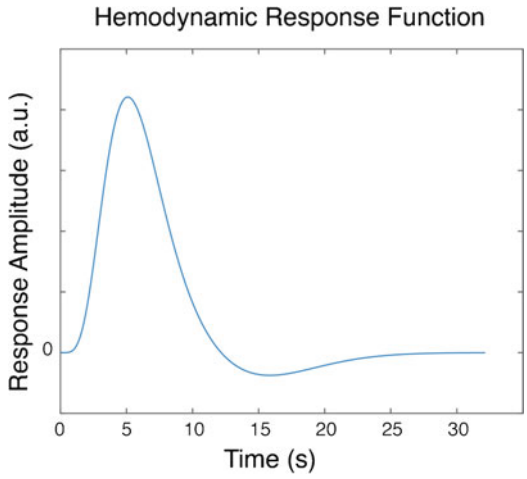

Fig. 11.7 Canonical hemodynamic response function

11.6 Event-Related and Block Design

The HRF can be used to predict how the BOLD response should look like at a location engaged in processing a stimulus (e.g., a flash of light) or performing a task (e.g., tapping a finger). The BOLD signal at each voxel can be compared with the HRF predicted response. If they are similar, the voxel is considered "activated"; otherwise, not. This strategy to localize brain activations, known as *statistical parametric mapping* [31], requires a careful experimental design alongside a rigorous statistical analysis. This section is focused on the experimental design, and the next section is focused on statistical analysis. We further confine the context of discussion to stimulus processing, while the same notion is readily generalizable to task performance.

Recall that HRF is the BOLD response to an impulse neural input. In other words, HRF itself is the prediction of the BOLD response given an impulse stimulus. A stimulus that lasts no more than 2 s is brief enough to be considered as an "event" or impulse, because HRF is slow and lasts over 25 s. To measure the event-related response, it is intuitive to design an experiment that includes discrete stimuli applied for many repetitions. Averaging the BOLD signal across the repeated events excludes the event-unrelated signal or noise and only yields the event-related response. Since the BOLD response is slow, the response to one event may overlap with the response to the next event, if they are not adequately separated in time. To avoid overlapping responses, the events should be repeated with an interval greater than 25 s or longer. This design, however, is inefficient because it has to prolong the experiment in order to include a sufficient number of events to obtain the event-related response with a high signal to noise ratio. An alternative design is to repeat events at random times such that the event-related response can be obtained by deconvolution, while the interval between adjacent events does not have to be long [28, 32]. For this type of *event-related design*, a specific strategy is to set the event timing according to an *M-sequence* [33], which is a pseudorandom sequence of ones and zeros with one indicating the presence of an event and zero indicating the absence of an event. The fact that the M-sequence has zero autocorrelation at any (non-zero) integer time shift prepares a nice precondition for the ease of deconvolution.

More common than the event-related design is the *block design*. In a block-design paradigm, stimuli are typically presented for a sustained period (or block), followed by a resting (or control) period that contains no stimulus (or only control stimuli). The stimulus-on block alternates with the stimulus-off block for multiple cycles. The ON block is often designed to have the same duration as the OFF block (but not always or necessarily the case), such that the paradigm can be described by a periodic boxcar function in which 1 means stimulus-on and 0 means stimulus-off. Prediction of the BOLD response is derived by convolving the boxcar function with the HRF. Typically, the on or off block lasts around 30 s such that the boxcar function has a characteristic frequency close to the peak frequency of the HRF in order to elicit the BOLD response with a relatively high signal to noise ratio. If the boxcar function has a much shorter period (i.e., a shorter ON or OFF block), the spectral characteristics of HRF limit the response amplitude and lower the signal to noise ratio.

11.7 BOLD Time Series Analysis

It follows that mapping brain activations is often achieved by analyzing the time series of each voxel with a model that depends on the experimental paradigm and HRF [31]. Specifically, the problem of activation mapping is formulated as a hypothesis test addressed separately for each voxel. For a given voxel, the null hypothesis is that the voxel is not activated by the stimulus/task paradigm; the alternative hypothesis is that it is activated. Herein, "activation" means the ability to predict the voxel time series with a response model (or design matrix), while the predictability is evaluated for statistical significance.

To elaborate, let us use a simple example in which visual stimuli are presented in a block-design paradigm (Fig. 11.8). This paradigm includes four resting blocks interleaved with three stimulation blocks; the resting and stimulation blocks are both 30 s. Given this paradigm, the response model sets up a prediction as to how the BOLD response should look like at a voxel activated by the stimulation. As aforementioned, the response model assumes that neurovascular coupling is a linear time-invariant system that can be described by the canonical HRF for every voxel in the brain. Given this assumption, the predicted response should look like a time series that results from temporal convolution of the 30 s-off-30 s-on boxcar function with the HRF.

Mathematically, let $s(t)$ be the function with which stimulation is applied, $h(t)$ be the HRF, and $x(t)$ be the regressor used to predict the fMRI response to the stimulation.

$$x(t) = s(t) * h(t) \tag{11.1}$$

The response model is simply a linear regression model, in which the same regressor is used to explain the BOLD signal at every voxel, denoted as $y_i(t)$ where i is the voxel index.

$$y_i(t) = \beta_i x(t) + b_i \tag{11.2}$$

The bias term, b_i, can be eliminated, if preprocessing is applied such that both $y_i(t)$ and $x(t)$ have their average (over time) equal to zero.

To address how well $y_i(t)$ is predictable by $x(t)$, one can simply evaluate the temporal correlation between $y_i(t)$ and $x(t)$ and test its statistical significance. The use of this simple correlation-based method can be dated back to a seminal paper by Bandettini et al., who were among the first to use fMRI to map activations (with a motor task) [9]. Although it is simple and effective, the correlation-based activation assessment is not applicable when the response model includes multiple regressors.

The need to use multiple regressors may arise in several scenarios. Perhaps the most intuitive one is when the experimental paradigm includes more than one type of stimuli. For example, we can use visual stimuli selective for the magnocellular (M) visual pathway in one stimulation block but the parvocellular (P) visual pathway in another stimulation block (Fig. 11.9). Then we need to include two regressors: one for M, $x_1(t)$, and the other for P, $x_2(t)$. The response model should be rewritten as below (note that the bias term is eliminated by preprocessing as mentioned earlier).

$$x_1(t) = s_1(t) * h(t) \tag{11.3}$$

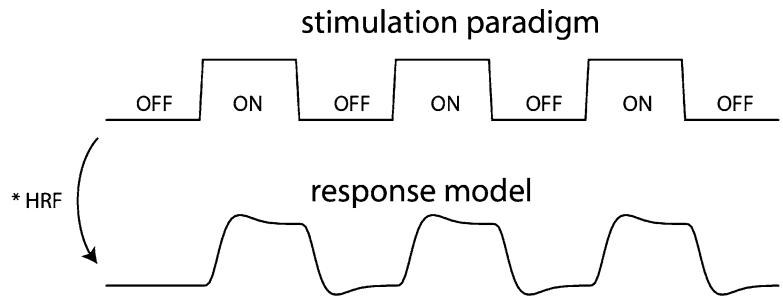

Fig. 11.8 Typical response model (bottom) given an ON-OFF block-design paradigm (top)

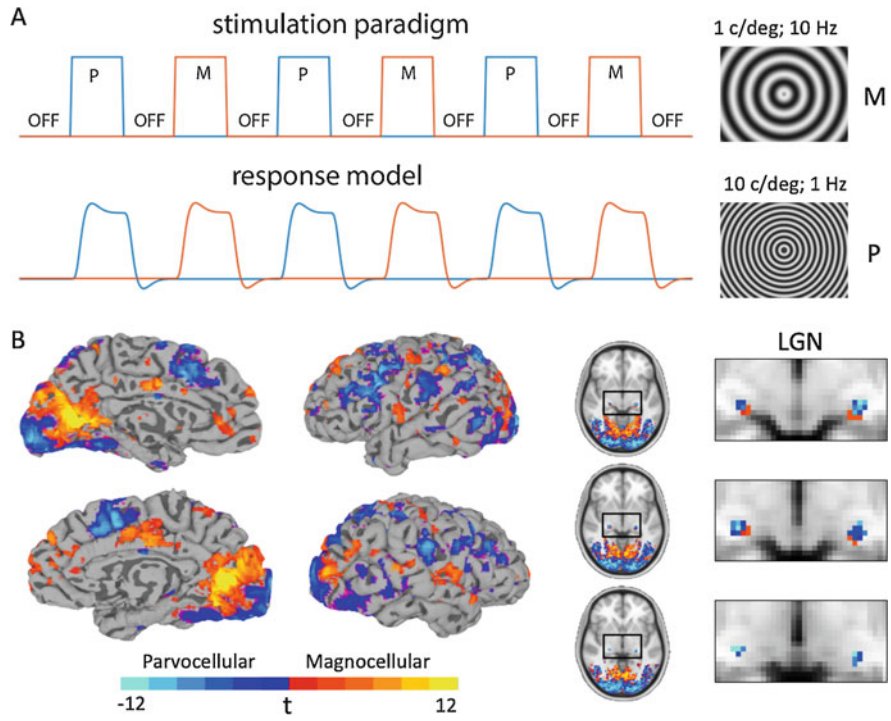

Fig. 11.9 Mapping magnocellular and parvocellular pathways. (**a**) A block-design paradigm involves two types of visual stimulation: one with high spatial frequency at 10 cycles per degree (c/deg) and low temporal frequency at 1 Hz and the other with low spatial frequency at 1 c/deg and high temporal frequency at 10 Hz, to selectively activate the magnocellular (M) and parvocellular (P) pathways in the visual system [34]. (**b**) The response contrast between the M- and P-selective stimuli is shown both on the cortical surface and in the brain volume. The contrast map segregates the M and P divisions in lateral geniculate nuclei (LGN) and their extensions onto (presumably) the dorsal and ventral streams on the cortex

$$x_2(t) = s_2(t) * h(t) \tag{11.4}$$

$$y_i(t) = \beta_{i1} x_1(t) + \beta_{i2} x_2(t) \tag{11.5}$$

The regression parameters (or beta values) can be estimated by least-squares estimation – an established method that has been implemented in many statistical analysis tools and has been elaborated in many statistical textbooks. Herein, we skip the details about the least-squares estimation and refer the readers interested to existing literature [31]. The estimated beta values, $\hat{\beta}_{i1}$ and $\hat{\beta}_{i2}$, can be further divided by their standard errors, $SE\left(\hat{\beta}_{i1}\right)$ and $SE\left(\hat{\beta}_{i2}\right)$, yielding the t statistics and the p values used to evaluate statistical significance regarding the BOLD activation associated with each stimulation condition or the contrast between conditions. See Fig. 11.9 for an example of using this strategy to separate the magnocellular and parvocellular divisions of the visual thalamus (i.e., lateral geniculate nuclei) and their extension onto the visual cortex.

In another scenario, one may use multiple regressors even when the experimental paradigm only includes one type of stimulation. Let us revisit how a regressor is defined. As in Eq. (11.1), the regressor results from convolving the boxcar function and the HRF, and it is assumed to be identical across voxel. What if the HRF is different from one location to another? This question is valid because the HRF is heuristic and neurovascular coupling may indeed vary across different brain regions (between the gray matter and the white matter, or between regions with distinct vascular density).

To accommodate the possible variation in HRF, one can express the HRF at each voxel as a Taylor's series of the canonical HRF.

$$h_i(t) = h(t) + \alpha_{i1} h'(t) + \alpha_{i2} h''(t) \quad (11.6)$$

Here, $h_i(t)$ is considered as a model of neurovascular coupling specific to the i-th voxel, and $h'(t)$ and $h''(t)$ are the first and second derivative of the canonical HRF. The coefficients, α_{i1} and α_{i2}, are unknown and assumed to be variable across locations in order to account for spatial variation in the HRF. Convolving the boxcar function with this voxel-wise HRF generates three regressors in the response model, as shown in Fig. 11.10.

$$x_1(t) = s(t) * h(t) \quad (11.7)$$

$$x_2(t) = s(t) * h'(t) \quad (11.8)$$

$$x_3(t) = s(t) * h''(t) \quad (11.9)$$

$$y_i(t) = \beta_{i1} x_1(t) + \beta_{i2} x_2(t) + \beta_{i3} x_3(t) \quad (11.10)$$

Note that the unknown coefficients, α_{i1} and α_{i2}, are considered as parts of the unknown beta values, which can be estimated from data by using least-squares estimation as discussed earlier. To evaluate the statistical significance, one only needs to evaluate the significance of the model as a whole (based on the F statistic) instead of the significance of each regressor (based on the t statistic), because all three regressors correspond to a single stimulus condition.

Lastly, let us place the problem in a different scenario, which has been overlooked in most fMRI studies but should, arguably, be considered. To understand this problem, let us recall that the HRF is a model of neurovascular coupling, describing how the neural response transforms to the BOLD response, given the external stimuli. Regressors used to predict the BOLD response should consider how neurons may differentially respond to the stimuli. In fact, evidence from neurophysiological studies suggests neural responses to a sustained period (e.g., 30 s) of stimulation may manifest themselves as a transient response at the onset of stimulation, a sustained response across the entire period of stimulation, a slow adaptation over the course of the stimulation pe-

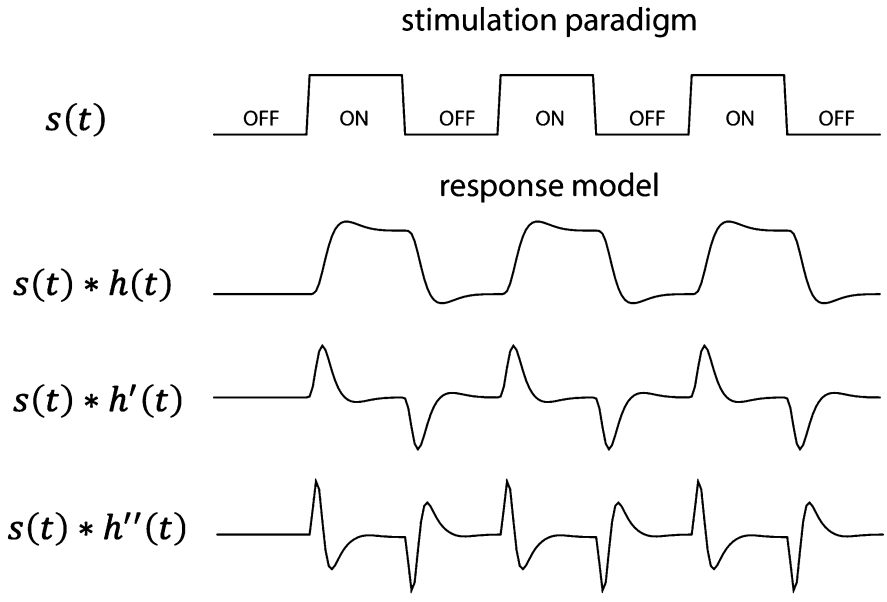

Fig. 11.10 Multiple regressors resulting from convolving the boxcar function with the canonical HRF, its first-order derivative, and its second-order derivative

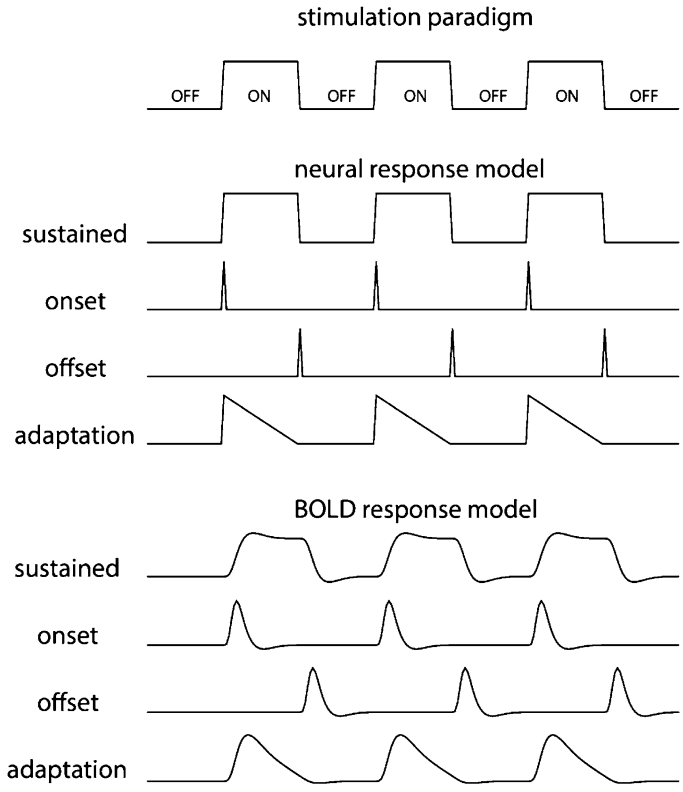

Fig. 11.11 Multiple regressors resulting from convolving sustained, onset, offset, and adaptation neural responses with the HRF, given a block-design paradigm

riod, a transient response at the offset of stimulation, or a mixture of these response features [35] (Fig. 11.11).

Equation (11.1) implies that we only consider the possibility of sustained neural response, which can be modeled as a boxcar function identical to the function that describes the stimulation. If we consider all four types of neural response that reflect the aforementioned onset, sustained, adaptation, and offset response, the response model should be revised as below.

$$x_1(t) = s(t) * h(t) \tag{11.11}$$

$$x_2(t) = s(t)\delta\,(t - \text{onset}) * h(t) \tag{11.12}$$

$$x_3(t) = s(t)\delta\,(t - \text{offset}) * h(t) \tag{11.13}$$

$$x_4(t) = s(t)\left(1 - \frac{t - \text{onset}}{\text{offset} - \text{onset}}\right) * h(t) \tag{11.14}$$

$$\mathrm{y}_i(t) = \beta_{i1}x_1(t) + \beta_{i2}x_2(t) + \beta_{i3}x_3(t) + \beta_{i4}x_4(t) \tag{11.15}$$

Although this model is more complex, it accommodates the variation of neural response and likely localizes different types of responses to different brain regions. See the example in Fig. 11.12.

The models discussed in this section are applicable to univariate analysis of BOLD time series. Being univariate means that the model is used to explain or predict the time series signal observed at each single voxel. It is in contrast to multivariate pattern analysis [36], for which the focus is on the activity pattern that spans multiple (typically neighboring) voxels. Moreover, the analysis discussed above is also limited to the signal observed from each single subject. The subject-level statistic can be used as the input to a second-level statistical test for evaluating the group-level significance.

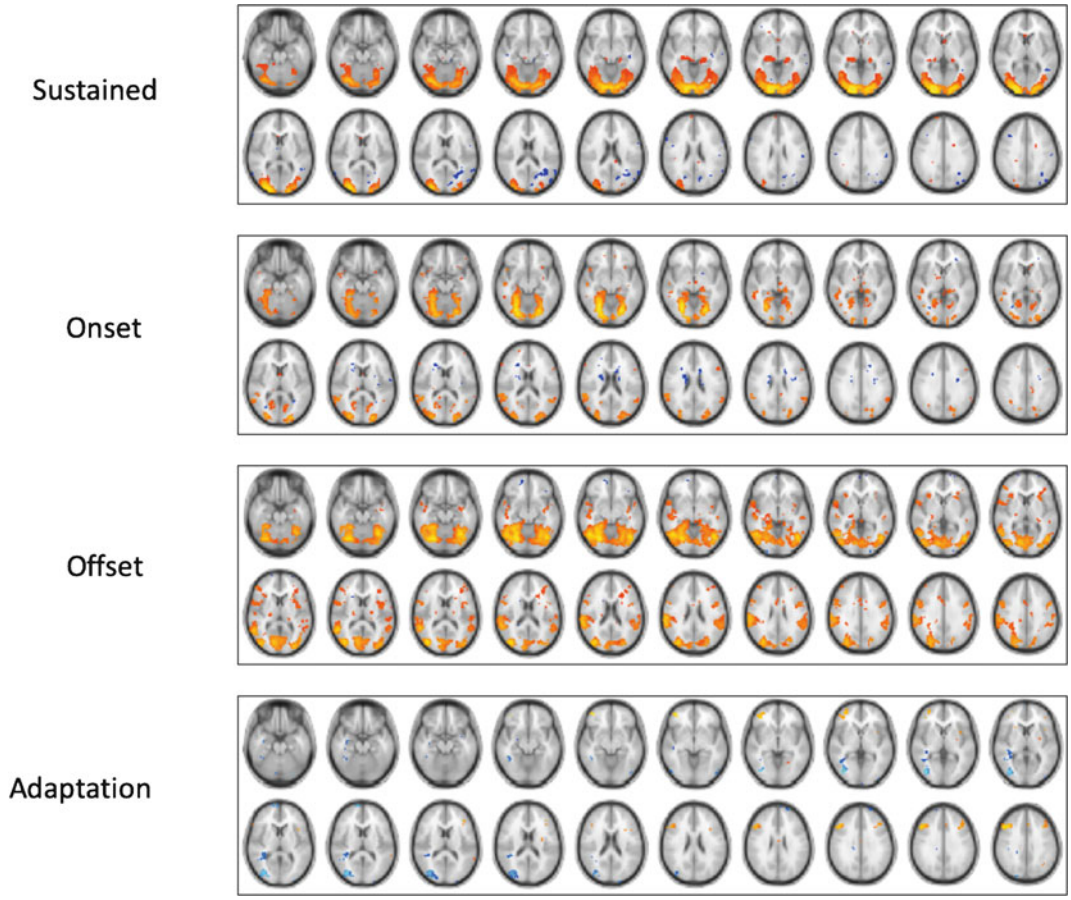

Fig. 11.12 BOLD activations corresponding to sustained, onset, offset, and adaptive responses to full-screen checkerboard stimulation in a block-design paradigm

11.8 Task fMRI for Functional Mapping

Based on the aforementioned experimental design and model-based analysis, fMRI has been widely used for functional mapping or localization. A function is exemplified by a specific task or stimulus. For example, pictures of human faces can be used as the visual stimulus presented in an event-related or block-design paradigm. The model-based time series analysis can be used to map the stimulus-evoked activation. The activation presumably highlights the brain regions involved in face recognition. One may also stimulate different body parts and map the resulting activations in the brain. This provides a way to localize the neural representation of each specific body part (see Fig. 11.13 for an example) and to further reveal the somatotopic organization. This strategy has been highly effective in mapping sensory, motor, and cognitive functions. The neuroscientific impact of task-based fMRI is significant, perhaps surpassing any prior method for functional mapping or localization for its noninvasiveness, ease of use, and high resolution. Clinical applications of task fMRI, however, remain challenging and limited, in part because interpretation of fMRI activations, although established in terms of statistics, is not straightforward as to how fMRI provides quantitative evidence to support neuropathological diagnosis or treatment planning.

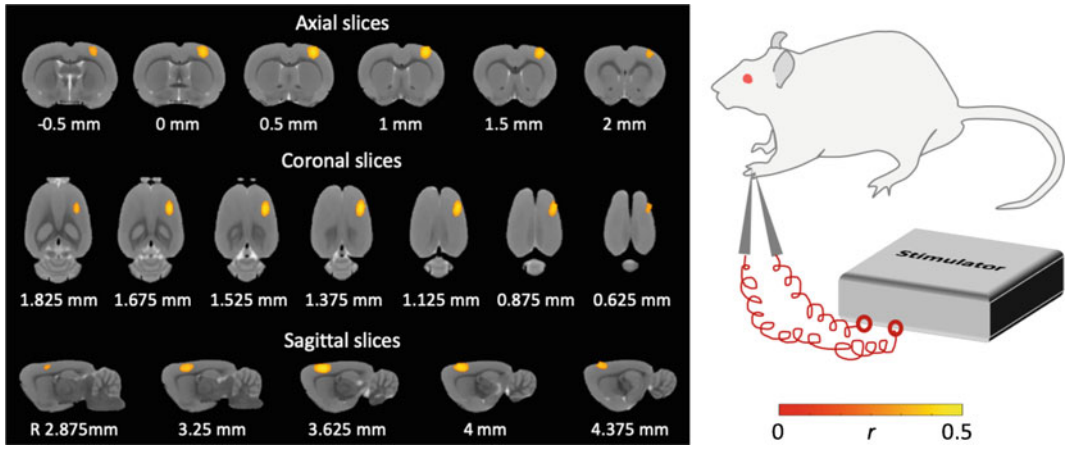

Fig. 11.13 In rats, BOLD fMRI activations with electrical stimulation applied to the forepaw

The value of fMRI has been most recognized for human psychological and cognitive sciences. It is worth noting that fMRI is also increasingly used in preclinical animal models. Animal fMRI has its unique value. With animals, it is much easier (and of less ethical concern) to combine fMRI with other invasive procedures. Combining fMRI with invasive neural recording or stimulation is desirable to reveal the relationship between fMRI and neurophysiology, uncover the physiological mechanism of fMRI, guide neuromodulation techniques for optimal effects on the brain, and evaluate the interaction between the brain and visceral organs, e.g., the gut. Therefore, animal fMRI plays an important role in brain research much beyond a backward translation from human fMRI and continues to be an area under active research.

11.9 Resting State fMRI

Even in the absence of any overt task, the brain is still active with spontaneous activity observable with BOLD fMRI [37]. The use of fMRI to measure and characterize brain activity in the resting state is referred to as *resting state fMRI*. As the name suggests, the resting state is not controlled by any task. Spontaneous activity is not driven by any predefined experimental paradigm, and it is thus not predictable by any task model that bears a simple functional interpretation. The statistical parametric mapping as described earlier is not readily applicable to resting state fMRI.

For resting state fMRI, an established method is so-called the seed-based correlation. It begins with selecting a region as the seed region and then calculating the correlation between the BOLD signal extracted from the seed region and the BOLD signal from every other voxel in the brain. The distribution of the resulting correlation coefficients highlights where in the brain spontaneous activity is temporally correlated with that at the seed region. Since temporal correlation is simply interpreted as functional connectivity, a term originally coined by Biswal et al. in his seminal paper [38], the map of correlation to a seed region is interpreted as a network, which includes all the regions that interact with the seed region. This seed-based correlation method is simple and effective and has been widely used to evaluate functional brain networks. To use this method, however, it requires one to select a seed region, presumably based on a specific question or hypothesis of interest. What if one does not have any question or hypothesis in mind? In this case, the seed region is likely subject to a somewhat arbitrary choice. In this case, such tools as InstaCorr implemented in AFNI would be helpful, since it allows one to explore any location as the seed region, while it calculates and visualizes the seed-based network nearly in real time.

Alternatively, an entirely data-driven method can be applied to uncover functional networks all at once without necessarily selecting any seed region as driven by a predefined hypothesis. Perhaps the most established method of this type is *independent component analysis* (ICA), or spatial ICA to be more specific [39]. For ICA, all voxels are considered altogether as elements of a high-dimensional input variable (or vector), and every time point is considered as a sample of this variable. The goal of ICA is to identify around tens of components, which are high-dimensional vectors that are mutually independent, while pushing their linear combination to be able to explain any sample of the input variable. In other words, any spatial pattern of resting state activity reflects an unknown but linear mixture of some fixed spatial patterns, each represented by an independent component. Collectively, these independent components capture the networks onto which voxels are organized (see Fig. 11.14 for an example). Learning algorithms to identify independent components from data, e.g., the Infomax algorithm [41], have been implemented in software tools, e.g., MELODIC in FSL. When ICA is applied to resting state fMRI data from a single subject, the resulting independent components can be inspected to identify and remove artifacts from signals in order to denoise the data. ICA can also be applied to data concatenated across a group of subjects, yielding group-level independent components that reflect functional network patterns consistent across subjects [42].

Although seed-based correlation and ICA are seemingly distinctive methods, they often end up with showing comparable spatial patterns [43]. These patterns are generally referred to as *resting state networks* and collectively depict the brain's functional organization, or brain connectome [44]. It is worth noting the resting state networks arising from spontaneous activity are consistent with patterns of brain activation with various tasks [45]. This consistency lends support to the functional relevance of resting state networks. However, the specific function of a resting state network is not always easy to elucidate, since it may or may not be associated with exteroceptive processes or human conscious cognition, for which one may design a relevant task for fMRI experiments. Some networks, such as the default-mode network [46], are intrinsic and preserved across brain states (wakefulness, sleep, anesthetized) and across many species (rat, monkey, human). Mapping resting state networks has become a mainstream focus for fMRI and holds the unique promise to facilitate further understanding and effective diagnosis of neurological disorders.

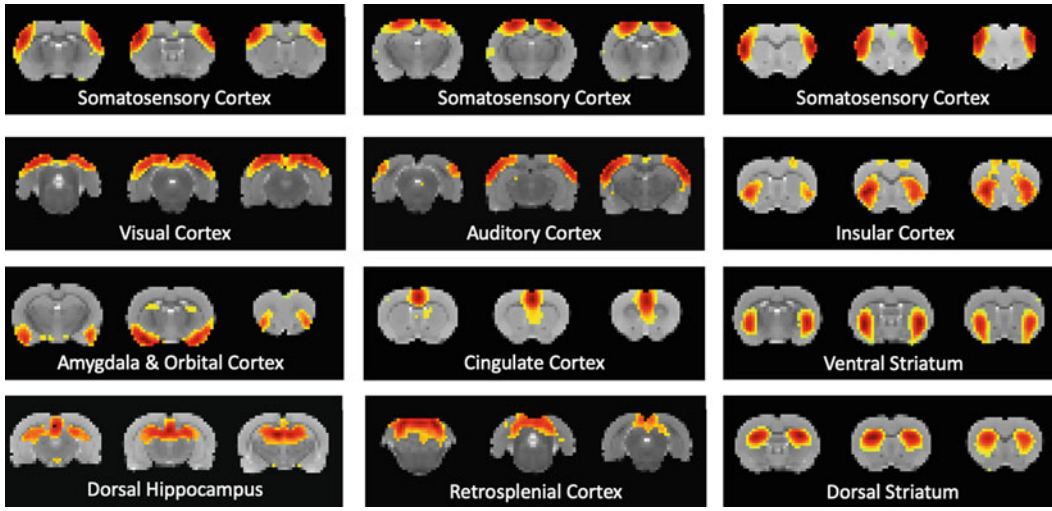

Fig. 11.14 Resting state networks obtained by applying ICA to fMRI data in rats. (Data are from Cao et al. [40])

11.10 Naturalistic Paradigm

Functional MRI is also increasingly used with naturalistic paradigms. Unlike event-related or block-design paradigms as discussed above, naturalistic paradigms set up a behavioral context much closer to our daily life experiences. For example, a natural visual paradigm may require a subject to watch a movie typically for 5–10 minutes. The movie often includes realistic scenes and objects, human or animal activity, and social content. Such a movie attracts attention, engages cognition, and activates the brain to a much greater extent than otherwise overly simplified visual stimuli as used in conventional fMRI studies. Similarly, a natural auditory paradigm may use continuous music or speech as stimuli [47, 48].

Natural visual or auditory stimulation is complex, because it involves many elements or features entangled in space, time, and frequency. Disentangling such features is seemingly unapproachable. The model-based analysis as used for event-related or block-design fMRI is not readily applicable to fMRI data obtained with naturalistic paradigms. Given natural stimuli, the fMRI signal appears nearly as irregular as spontaneous activity observed with resting state fMRI. Seemingly, no tangible clue is easily accessible to separate stimulus-driven responses from spontaneous activity.

The dilemma is resolved, partially, with the finding first reported by Hasson et al. In their seminal paper [49], evidence reported suggests that naturalistic stimuli, either a movie or an audio story, elicit highly reproducible responses within and across subjects. When a human subject watches the same movie twice (in two repeated sessions), the responses observed in the first session and the second session are significantly correlated for each voxel involved in processing the information from the movie. When two subjects watch the same movie, the responses observed from the first and second subjects are also highly correlated for each activated voxel. This finding lends support to a simple method that allows us to map brain activation with natural stimuli by evaluating the voxel-wise intra/inter-subject reproducibility of the fMRI signal. The high reproducibility is unique to the fMRI signal during natural stimuli and not observable given seemingly complex and irregular stimuli that are perceptually meaningless [50]. This method is robust, effective, and model-free, extending the application of fMRI to ecologically relevant scenarios.

The fact that brain responses to natural stimuli are significantly reproducible within and across subjects can be utilized to map functional networks engaged in processing natural stimuli. For this purpose, we may use inter-session or inter-subject functional connectivity analysis [51]. Specifically, when a human subject watches the same movie twice, we can choose a seed region, extract its signal from the first session, and calculate its correlation with the signal from every voxel in the second session [52]. The inter-session functional connectivity is only attributable to stimulus-driven responses instead of spontaneous activity, which is unrelated to stimuli and thus unlikely to be correlated between two separate sessions. Similarly, one may apply this analysis to data from two subjects watching the same movie, yielding inter-subject functional connectivity also indicative of stimulus-driven functional networks.

The methods described above are compelling because of their simplicity. Nevertheless, it should be noted that the correlation-based measures of inter-subject/inter-session reproducibility reveal only where in the brain is involved in processing natural stimuli, but not how an activated voxel is involved or what information it encodes. To answer these questions, we should address the stimulus-response relationship (or neural coding) at each voxel [53]. As mentioned earlier, the complexity of natural stimuli requires a model to be able to unpack the stimuli into candidate features, which are individually or collectively represented by a voxel. Although it remains to be fully developed, a promising method, as advocated in recent studies [54–56], is to use brain-inspired deep neural networks as feature models to address neural coding with natural stimuli.

The use of natural visual or auditory stimuli is emerging as a new paradigm for fMRI. It places

new challenges and opportunities for using fMRI not only to assign functions to regions (functional localization) but also to uncover the computational role of individual locations, regions, or networks (i.e., neural coding or representation) in a realistic and dynamic condition being one step closer to our daily life.

11.11 Summary

To recap, we list the following points in summary.

- fMRI is based on MRI of hydrogen protons.
- Transverse relaxation following on-resonance RF excitation depends on T_2*.
- Hemoglobin is diamagnetic when oxygenated but paramagnetic when deoxygenated.
- Increase in the concentration of deoxygenated hemoglobin shortens T_2*.
- The bold oxygenation level–dependent signal is the vascular response to neural activity.
- Neural activation increases regional cerebral metabolic rate of oxygen ($CMRO_2$), triggers vessel dilation, and increases regional cerebral blood flow (CBF) and cerebral blood volume (CBV).
- Increase in CBF overcompensates $CMRO_2$ and raises the blood oxygenation level.
- Neural activation increases the BOLD signal.
- fMRI uses the BOLD signal to localize neural activations, despite the incomplete understanding of the BOLD mechanism.
- HRF describes neurovascular coupling as a linear time-invariant system.
- HRF reflects the BOLD response to an impulse neural response, or an impulse stimulus.
- Task fMRI typically uses event-related or block-design paradigms.
- To map or localize activation, the BOLD signal is compared against a response model derived from the experimental paradigm and the HRF.
- A voxel is activated by a stimulus or task, if its time series is predictable by the response model.
- Resting state fMRI measures spontaneous brain activity in the absence of any overt task.
- Seed-based correlation or independent component analysis can be used to map resting state networks.
- Brain activation evoked by naturalistic stimuli can be mapped by evaluating intra/inter-subject reproducibility of the BOLD signal observed during two separate sessions of the same stimuli.
- Brain networks evoked by naturalistic stimuli can be mapped by evaluating intra/inter-subject functional connectivity with the BOLD signal observed during two separate sessions of the same stimuli.

Homework

Please mark all the correct answers for each of the following questions. Note that each question may have one or more than one correct answer.

1. Which of the following nuclei is the most abundant for functional magnetic resonance imaging?
   (A) ^{1}H
   (B) ^{13}C
   (C) ^{31}P
   (D) ^{19}F
2. Hydrogen protons spin at about 300 MHz in a 7 Tesla MRI system. Which of the following is close to the gyromagnetic ratio (MHz T^{-1}) of ^{1}H spins?
   (A) 42.6
   (B) 6.53
   (C) 40.1
   (D) 11.3
3. Which of the following are true about on-resonance RF excitation?
   (A) It transmits an oscillating magnetic field along the longitudinal direction.
   (B) It transmits an oscillating magnetic field in the transverse plane.
   (C) It transmits an oscillating magnetic field with a frequency that matches the Larmor frequency of the target spin systems.

(D) It transmits energy to be effectively absorbed by the target spin systems.

4. Which of the following contribute to the blood oxygenation level-dependent contrast?
   (A) Cerebral blood flow
   (B) Cerebral blood volume
   (C) Cerebral metabolic rate of oxygen
   (D) Myelin density
5. Which of the following regional changes occur accompanying local neural activation?
   (A) Arterioles dilate
   (B) Blood flow increases
   (C) Oxygen consumption increases
   (D) Blood oxygenation level increases
6. What happens when the concentration of deoxy-hemoglobin increases?
   (A) Transverse relaxation becomes faster
   (B) Transverse magnetization decays faster
   (C) Longitudinal relaxation becomes faster
   (D) Longitudinal magnetization recovers faster
7. Which of the following are TRUE about the hemodynamic response function (HRF)?
   (A) It indicates the hemodynamic response given an impulse input stimulus
   (B) It indicates the hemodynamic response given a sustained block of input stimulus
   (C) In HRF, the peak response delays from the time zero
   (D) In HRF, the peak response precedes the time zero
8. How fast is the fMRI signal typically sampled?
   (A) Every millisecond
   (B) Every second
   (C) Every minute
   (D) Every hour
9. To derive the response model (or design matrix) for the BOLD time series analysis, one needs to
   (A) Convolve the stimulus paradigm with the hemodynamic response function
   (B) Multiply the stimulus paradigm with the hemodynamic response function
   (C) Add the stimulus paradigm with the hemodynamic response function
   (D) None of the above
10. In the block design, what would be a typical block duration?
    (A) 30 seconds ON vs. 30 seconds OFF
    (B) 30 milliseconds ON vs. 30 milliseconds OFF
    (C) 30 minutes ON vs. 30 minutes OFF
    (D) None of the above
11. Which of the following are TRUE about resting state fMRI?
    (A) It is used to report instrumental noises from the MRI scanner
    (B) It is used to measure spontaneous brain activity in the absence of overt tasks or stimuli
    (C) It is used to measure fluctuations in membrane potentials around -70 mV
    (D) None of the above
12. Functional connectivity as observed with resting state fMRI refers to?
    (A) Temporal correlations between the signals observed from different brain locations
    (B) Anatomical connections between different brain locations
    (C) The relationship between neural and vascular signals in the brain
    (D) None of the above
13. When applied to resting state fMRI data, independent component analysis
    (A) Separates brain networks without specifying a seed location
    (B) Assumes brain networks are spatially independent of one another
    (C) Shows where in the brain is at rest
    (D) None of the above
14. To map brain activations with a continuous period of naturalistic stimuli, one can
    (A) Calculate the voxel-wise correlation between the fMRI signals from a subject during two repeated sessions of the same stimuli
    (B) Calculate the voxel-wise correlation between the fMRI signals from two subjects during the same stimuli
    (C) Use a response model derived from convolving a boxcar function with the canonical HRF

(D) Calculate the seed-based correlation based on the fMRI signals recorded from a single session

References

1. B. He, Z. Liu, Multimodal functional neuroimaging: Integrating functional MRI and EEG/MEG. IEEE Rev. Biomed. Eng. **1**, 23–40 (2008)
2. R.W. Brown, Y.-C. Cheng, M.E. Haack, M.R. Thompson, R. Venkatesan, *Magnetic Resonance Imaging: Physical Principles and Sequence Design*, 2nd edn. (Wiley, Hoboken, New Jersey, 2014)
3. S.A. Huettel, A.W. Song, G. McCarthy, *Functional Magnetic Resonance Imaging*, 3rd edn. (Oxford University Press, 2014)
4. Z.-P. Liang, P.C. Lauterbur, *Principles of Magnetic Resonance Imaging: A Signal Processing Perspective* (IEEE Press, 1999)
5. S. Ogawa, T.M. Lee, A.R. Kay, D.W. Tank, Brain magnetic resonance imaging with contrast dependent on blood oxygenation. PNAS **87**(24), 9868–9872 (1990)
6. L. Pauling, C.D. Coryell, The magnetic properties and structure of hemoglobin, oxyhemoglobin and carbonmonoxyhemoglobin. PNAS **22**(4), 210–216 (1936)
7. K.R. Thulborn, J.C. Waterton, P.M. Matthews, G.K. Radda, Oxygenation dependence of the transverse relaxation time of water protons in whole blood at high field. Biochim. Biophys. Acta **714**(2), 265–270 (1982)
8. R. Turner, D. Le Bihan, C.T.W. Moonen, D. Despres, J. Frank, Echo-planar time course MRI of cat brain oxygenation changes. Magn. Reson. Med. **22**(1), 159–166 (1991)
9. P.A. Bandettini, E.C. Wong, S.R. Hinks, R.S. Tikofsky, J.S. Hyde, Time course EPI of human brain function during task activation. Magn. Reson. Med. **25**(2), 390–397 (1992)
10. K.K. Kwong, J.W. Belliveau, D.A. Chesler, I.E. Goldberg, R.M. Weisskoff, B.P. Poncelet, D.N. Kennedy, B.E. Hoppel, M.S. Cohen, R. Turner, Dynamic magnetic resonance imaging of human brain activity during primary sensory stimulation. Proc. Natl. Acad. Sci. U S A **89**(12), 5675–5679 (1992)
11. S. Ogawa, D.W. Tank, R. Menon, J.M. Ellermann, S.-G. Kim, H. Merkle, K. Ugurbil, Intrinsic signal changes accompanying sensory stimulation: Functional brain mapping with magnetic resonance imaging. PNAS **89**(13), 5951–5955 (1992)
12. R.B. Buxton, The physics of functional magnetic resonance imaging. Rep. Prog. Phys. **76**(9), 096601 (2013)
13. S.-G. Kim, S. Ogawa, Biophysical and physiological origins of blood oxygenation level dependent fMRI signals. J. Cereb. Blood Flow Metab. **32**(7), 1188–1206 (2012)
14. R.B. Buxton, E.C. Wong, L.R. Frank, Dynamics of blood flow and oxygenation changes during brain activation: The balloon model. Magn. Reson. Med. **39**(6), 855–864 (1998)
15. P.T. Fox, M.E. Raichle, Focal physiological uncoupling of cerebral blood flow and oxidative metabolism during somatosensory stimulation in human subjects. PNAS **83**(4), 1140–1144 (1986)
16. M.K. Stehling, R. Turner, P. Mansfield, Echo-planar imaging: Magnetic resonance imaging in a fraction of a second. Science **254**(5028), 43–50 (1991)
17. G.H. Glover, Spiral imaging in fMRI. NeuroImage **62**(2), 706–712 (2012)
18. D.C. Noll, J.D. Cohen, C.H. Meyer, W. Schneider, Spiral k-space MR imaging of cortical activation. J. Magn. Reson. Imaging **5**(1), 49–56 (1995)
19. S. Moeller, E. Yacoub, C.A. Olman, E. Auerbach, J. Strupp, N. Harel, K. Ugurbil, Multiband multislice GE-EPI at 7 tesla, with 16-fold acceleration using partial parallel imaging with application to high spatial and temporal whole-brain fMRI. Magn. Reson. Med. **63**(5), 1144–1153 (2010)
20. K. Setsompop, B.A. Gagoski, J.R. Polimeni, T. Witzel, V.J. Wedeen, L.L. Wald, Blipped-controlled aliasing in parallel imaging for simultaneous multislice echo planar imaging with reduced g-factor penalty. Magn. Reson. Med. **67**(5), 1210–1224 (2012)
21. N.K. Logothetis, What we can do and what we cannot do with fMRI. Nature **453**(12), 869–883 (2008)
22. G.C. Petzold, V.N. Murthy, Role of astrocytes in neurovascular coupling. Neuron **71**(5), 782–797 (2011)
23. N.K. Logothetis, J. Pauls, M. Augath, T. Trinath, A. Oeltermann, Neurophysiological investigation of the basis of the fMRI signal. Nature **412**, 150–157 (2001)
24. Z. Ding, Y. Huang, S.K. Bailey, Y. Gao, L.E. Cutting, B.P. Roger, A.T. Newton, J.C. Gore, Detection of synchronous brain activity in white matter tracts at rest and under functional loading. PNAS **115**(3), 595–600 (2018)
25. J.R. Gawryluk, E.L. Mazerolle, R.C. D'Arcy, Does functional MRI detect activation in white matter? A review of emerging evidence, issues, and future directions. Front. Neurosci. **8**, 239 (2014)
26. L. Marussich, K.-H. Lu, H. Wen, Z. Liu, Mapping white-matter functional organization at rest and during naturalistic visual perception. NeuroImage **146**, 1128–1141 (2017)
27. G.M. Boynton, S.A. Engel, G.H. Glover, D.J. Heeger, Linear systems analysis of functional magnetic resonance imaging in human V1. J. Neurosci. **16**(13), 4207–4221 (1996)
28. G.H. Glover, Deconvolution of impulse response in event-related BOLD fMRI. NeuroImage **9**(4), 416–429 (1999)
29. J. Cao, K.-H. Lu, S.T. Oleson, R.J. Phillips, D. Jaffey, C.L. Hendren, T.L. Powley, Z. Liu, Gastric stimulation drives fast BOLD responses of neural origin. NeuroImage **197**, 200–211 (2019)

30. L.D. Lewis, K. Setsompop, B.R. Rosen, J.R. Polimeni, Fast fMRI can detect oscillatory neural activity in humans. PNAS **113**(43), E6679–E6685 (2016)
31. K.L. Friston, A.P. Holmes, K.J. Worsley, J.-P. Poline, C.D. Frith, R.S.J. Frackowiak, Statistical parametric maps in functional imaging: A general linear approach. Hum. Brain Mapp. **2**(4), 189–210 (1994)
32. T.T. Liu, The development of event-related fMRI designs. NeuroImage **62**(2), 1157–1162 (2012)
33. G.T. Buracas, G.M. Boynton, Efficient design of event-related fMRI experiments using M-sequences. NeuroImage **16**, 801–813 (2002)
34. A.M. Derrington, P. Lennie, Spatial and temporal contrast sensitivities of neurones in lateral geniculate nucleus of macaque. J. Physiol. **357**, 219–240 (1984)
35. E. Duff, J. Xiong, B. Wang, R. Cunnington, P.T. Fox, G. Egan, Complex spatio-temporal dynamics of fMRI BOLD: A study of motor learning. NeuroImage **34**(1), 156–168 (2007)
36. N. Kriegeskorte, R. Goebel, P.A. Bandettini, Information-based functional brain mapping. PNAS **103**(10), 3863–3868 (2006)
37. M.D. Fox, M.E. Raichle, Spontaneous fluctuations in brain activity observed with functional magnetic resonance imaging. Nat. Rev. Neurosci. **8**, 700–711 (2007)
38. B. Biswal, F.Z. Yetkin, V.M. Haughton, J.S. Hyde, Functional connectivity in the motor cortex of resting human brain using echo-planar MRI. Magn. Reson. Med. **34**(4), 537–541 (1995)
39. C.F. Bechmann, M. DeLuca, J. Devlin, S.M. Smith, Investigation into resting-state connectivity using independent component analysis. Philos. Trans. R. Soc. B **360**(1457), 1001–1013 (2005)
40. J. Cao, K.-H. Lu, T.L. Powley, Z. Liu, Vagal nerve stimulation triggers widespread responses and alters large-scale functional connectivity in the rat brain. PLoS One **12**(12), e0189518 (2017)
41. A.J. Bell, T.J. Sejnowski, An information-maximization approach to blind separation and blind deconvolution. Neural Comput. **7**(6), 1129–1159 (1995)
42. V.D. Calhoun, J. Liu, T. Adali, A review of group ICA for fMRI data and ICA for joint inference of imaging, genetic, and ERP data. NeuroImage **45**, S163–S172 (2009)
43. K.R.A. Van Dijk, T. Hedden, A. Venkataraman, K.C. Evans, S.W. Lazar, R.L. Buckner, Intrinsic functional connectivity as a tool for human connectomics: Theory, properties, and optimization. J. Neurophysiol. **103**(1), 297–321 (2010)
44. D.C. Van Essen, S.M. Smith, D.M. Barch, T.E.J. Behren, E. Yacoub, K. Ugurbil, The WU-Minn human connectome project: An overview. NeuroImage **80**, 62–79 (2013)
45. S.M. Smith, P.T. Fox, K.L. Miller, D.C. Glahn, M.P. Fox, C.E. Mackay, N. Filippini, K.E. Watkins, R. Toro, A.R. Laird, C.F. Beckmann, Correspondence of the brain's functional architecture during activation and rest. PNAS **106**(31), 13040–13045 (2009)
46. M.E. Raichle, The Brain's default mode network. Annu. Rev. Neurosci. **38**, 433–447 (2015)
47. Y. Zhang, G. Chen, H. Wen, K.-H. Lu, Z. Liu, Musical imagery involves Wernicke's area in bilateral and anti-correlated network interactions in musicians. Sci. Rep. **7**(17066), 2017 (2017)
48. Y. Zhang, K. Han, R.M. Worth, Z. Liu, Connecting concepts in the brain by mapping cortical representations of semantic relations. biorxiv, https://doi.org/10.1101/649939 (2019)
49. U. Hasson, Y. Nir, I. Levy, G. Fuhrmann, R. Malach, Intersubject synchronization of cortical activity during natural vision. Science **303**(5664), 1634–1640 (2004)
50. K.-H. Lu, S. Hung, H. Wen, L. Marussich, Z. Liu, Mapping white-matter functional organization at rest and during naturalistic visual perception. PLoS One **11**(8), e0161797 (2016)
51. E. Simony, C.J. Joney, J. Chen, O. Losiksky, Y. Yeshurun, A. Wiesel, U. Hasson, Dynamic reconfiguration of the default mode network during narrative comprehension. Nat. Commun. **7**, 12141 (2016)
52. L.K. Lynch, K.-H. Lu, H. Wen, Y. Zhang, A.J. Saykin, Z. Liu, Task-evoked functional connectivity does not explain functional connectivity differences between rest and task conditions. Hum. Brain Mapp. **39**(12), 4939–4948 (2018)
53. T. Naselaris, K.N. Kay, S. Nishimoto, J.L. Gallant, Encoding and decoding in fMRI. NeuroImage **56**(2), 400–410 (2011)
54. M. Eickenberg, V.G. Gramfort, B. Thirion, Seeing it all: Convolutional network layers map the function of the human visual system. NeuroImage **152**, 184–194 (2017)
55. U. Güçlü, M.A.J. van Gerven, Deep neural networks reveal a gradient in the complexity of neural representations across the ventral stream. J. Neurosci. **35**(27), 100005–110014 (2015)
56. H. Wen, J. Shi, Y. Zhang, K.-H. Lu, J. Cao, Z. Liu, Neural encoding and decoding with deep learning for dynamic natural vision. Cereb. Cortex **28**(12), 4136–4160 (2018)